

An Intelligent Algorithm Based on the Improved CNN-LSTM for the Detection of Concrete Reinforcement Information

Xuefeng Bai¹, Ronghua Zhang^{2,*}, Jinxun Le², Boyang Li¹, Wenying Fu², Shuqing Jia², and Wuliang Yin³

¹*School of Control Science and Engineering, Tiangong University, Tianjin 300387, China*

²*School of Artificial Intelligence, Tiangong University, Tianjin 300387, China*

³*School of Engineering, The University of Manchester, M13 9PL, UK*

ABSTRACT: Reinforced concrete plays a vital role in the construction industry. Therefore, it is necessary to evaluate the parameters such as the number, diameter, and protective layer thickness of rebar in concrete during and after the construction process. In this paper, we take the pulsed eddy current detection method as the principle, build the relevant experimental system, collect the data samples about the parameter information of the rebar, and propose an intelligent algorithm based on Convolutional Neural Network with Long Short-Term Memory (CNN-LSTM) based on Convolutional Block Attention Module (CBAM), which is capable of automatically extracting the relevant features of information-rich PECT signals, and the CBAM is introduced into CNN to enhance its feature extraction capability, which improves the accuracy and interpretability of CBAM-CNN-LSTM in predicting rebar information. In order to verify the performance of the method, traditional CNN, LSTM, and CNN-LSTM algorithms were used for comparison, and the prediction results were evaluated by the decision coefficient (R^2), Explained Variance Score (EVS), Root Mean Square (RMSE), and Mean Absolute Error (MAE). The experimental results show that the method is able to accurately predict the specimen information with good prediction accuracy and stability as the average error of the prediction of the number is reduced by 50% and the average error of diameter and thickness prediction reduced by 20% and 3% after adding the CBAM.

1. INTRODUCTION

Reinforced Concrete (RC) structures are widely used in the construction industry because of their high strength, design flexibility, long service life, and low cost. Since the quality of reinforcement in concrete plays a key role in the overall quality of the building structure, it is crucial to test the diameter, quantity, and thickness of the protective layer of rebar during the construction process. At present, Non-Destructive Testing (NDT) is favoured by scholars, experts, and testing engineers because it does not cause any damage to the object to be tested in the testing process [1]. Instead, it involves an indirect testing of the object by observing changes in physical or chemical reactions caused by its structural abnormalities. Among them, Radiographic Testing (RT) [2], Infrared Thermographic Testing (INT) [3, 4], Radio Detection and Ranging (RADAR) [5, 6], and Eddy Current Testing (ECT) [7] can be used as methods for NDT of reinforcing steel. Although the former three detection methods have advantages such as high precision and visualisation of detection results, they all have drawbacks such as high detection costs, complex operation, and a certain degree of harm to the surrounding environment and operators. Compared with these methods, ECT is one of the most suitable methods for rebar measurement due to its low cost, easy operation, and high accuracy in detecting results [8]. Pulsed eddy current testing (PECT) is an important branch of ECT. Compared with ECT, PECT has the advantages of rich frequency components,

stronger penetration ability, and the ability to balance the depth of detection and accuracy. Its operating principle is the Law of Electromagnetic Induction, which obtains the information about the object being measured through the amount of change in the voltage of the detector coil or changes in the magnetic field [9, 10].

However, the main challenge in rebar detection using PECT technology is the inverse solution required to extract information about the tested parts from the detection data. Due to the close proximity of multiple reinforcement bars, as well as improper or uneven concrete pouring, some problems are easy to appear such as steel deviation, high and low positions of steel bars. These issues can impact the detection values in actual measurements. The inverse solution algorithm is challenging as it needs to extract various features from numerous relevant detection values and provide accurate information about the specimen. At present, the anti-solution algorithm is roughly divided into two types: one is the database matching method. The relevant data on various operating conditions are collected through field measurements. Subsequently, a database is established in the Microcontroller Unit (MCU) to make the detection value correspond to the information of the rebars. This method requires a large amount of data collection in the early stages to support the establishment of the database. At the same time, the applicability is low. The same set of databases is not applicable to all reinforced concrete. The other is the traditional neural network method. Machine learning methods such as Back Propagation (BP) neural networks and Support Vector Machine

* Corresponding author: Ronghua Zhang (rh_zhang_2005@163.com).

(SVM) are used to interpret reinforced concrete data [11, 12]. These methods establish a nonlinear mapping between the detection values and the information of rebar diameter and thickness. On one hand, the process of manually extracting features is both laborious and time-consuming. On the other hand, this approach could result in the loss of vital information when extracting features manually, and these drawbacks are often unavoidable in machine learning applications. However, deep learning can be applied to the RC detection process for better automation and efficiency. It can automatically learn features directly from raw data in an end-to-end manner, eliminating the need for manual feature extraction and rule definition [13].

In recent years, many scholars have combined various types of traditional models and made full use of their respective advantages, thus enhancing the performance of the overall model. For example, in medical field, Petmezas et al. [14] proposed combining Convolutional Neural Network with Long Short-Term Memory (CNN-LSTM) models to accurately detect atrial fibrillation in ECG examinations. In industrial field, Elmaz et al. [15] predicted indoor temperature modeling using a black-box CNN-LSTM architecture and compared its performance with Multilayer Perceptron (MLP) and LSTM. CNN-LSTM outperformed all other models in all prediction ranges and showed better robustness to error accumulation. Kim et al. [16] designed a model for predicting energy consumption in housing using CNN-LSTM neural networks. They analyzed and identified the factors that have the most significant impact on predicting electricity consumption. In the area of time series forecasting, Hou et al. [17] used a CNN-LSTM network model to forecast future hourly temperatures. Yan et al. [18] proposed the use of CNN, LSTM, and CNN-LSTM based on spatiotemporal clustering to establish a multi-time, multi-site forecasting model of Beijing's air quality and to compare them with a back-propagation neural network (BPNN). Nevertheless, the magnitude of the detection signal is related to the distance from the rebar in this paper, which is a dynamic process. In other words, the signal value increases as the distance decreases. Therefore, the collection of a series of test values can also be considered as time-series data, and in the above literature, Convolutional Neural Network (CNN) has demonstrated excellent feature extraction of raw data, while Long Short-Term Memory (LSTM) networks have shown the ability to capture time-series information and long-term dependencies [15, 19]. In this paper, a network architecture based on CNN-LSTM with Convolutional Block Attention Module (CBAM) [20] is proposed for automatic prediction of rebar information. The network primarily consists of CBAM, CNN, and LSTM. CNNs are initially employed to automatically extract features from the rebar signal data. However, CNNs can only extract features through convolution and pooling operations. As a result, they do not automatically focus on the importance of different channels and spatial locations. They focus solely on local information and lack the full use of global contextual information effectively. CBAM has the advantage of increasing the importance of each channel and location, using global information to enhance feature representation capability [20]. Therefore, CBAM is chosen to compensate the shortcomings during conventional CNN feature extraction. Finally, the extracted features are fed into

the LSTM to learn temporal correlation properties for prediction. It has been experimentally verified that the proposed network model has good prediction and generalization capabilities. Finally, the remaining sections of this paper are as follows. Section 2 describes the experimental system and samples. Section 3 details the overall structure of CBAM-CNN-LSTM and the role of each component. Section 4 analyzes and discusses the experimental results. Finally, Section 5 provides conclusion.

2. EXPERIMENTAL SYSTEMS AND SAMPLES

2.1. PECT System

The detection principle model is shown in Fig. 1. When the excitation coil is pulsed, the alternating current I_1 causes a rapid decay of the magnetic field B_1 . The downward propagation of B_1 will be interrupted by the magnetic inductance line when it encounters the rebars, resulting in the generation of transient eddy currents I_2 on the surface, which produces the opposite transient magnetic field B_2 . The magnitude of B_2 is related to the magnitude of the eddy currents and depends on the physical factors of the conductor specimen under test, such as magnetic permeability, electrical conductivity, size, and shape. Simultaneously, it is also associated with the distance from the specimen to the coil and the excitation frequency of the excitation coil. Finally, the equivalent impedance of the excitation coil is influenced by the reverse magnetic field B_2 , which is then converted into a voltage output for detection by the detection coil.

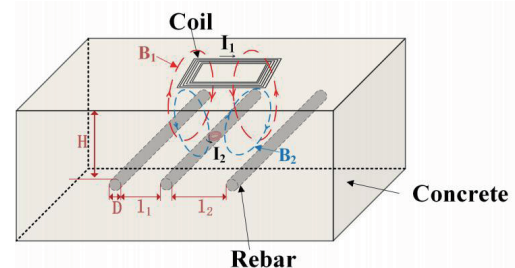


FIGURE 1. PECT principle model diagram.

The diagram of the experiment in this study is shown in Fig. 2(a), and the PECT detection system mainly consists of four components, including rectangular coil array type sensors, power amplifier circuit, signal conditioning module, and data acquisition module. Based on the directional nature of rectangular coils and their capability to produce a uniform distribution of eddy currents, along with the geometry of the object being measured, the rebar can be easily positioned [21]. The sensor part consists of one excitation coil and four detection coils independently. The specific sensor parameters are shown in Table 1.

As shown in Fig. 2(b), the experimental procedure began with the use of the square wave signal from the FY6300 signal generator to drive the coil. The square wave signal is set to have a duty cycle of 50%, an amplitude of 5 V, a rise time of 1 μ s, and a frequency of 200 Hz. Since the maximum current output from the signal generator is only mA, which is in-

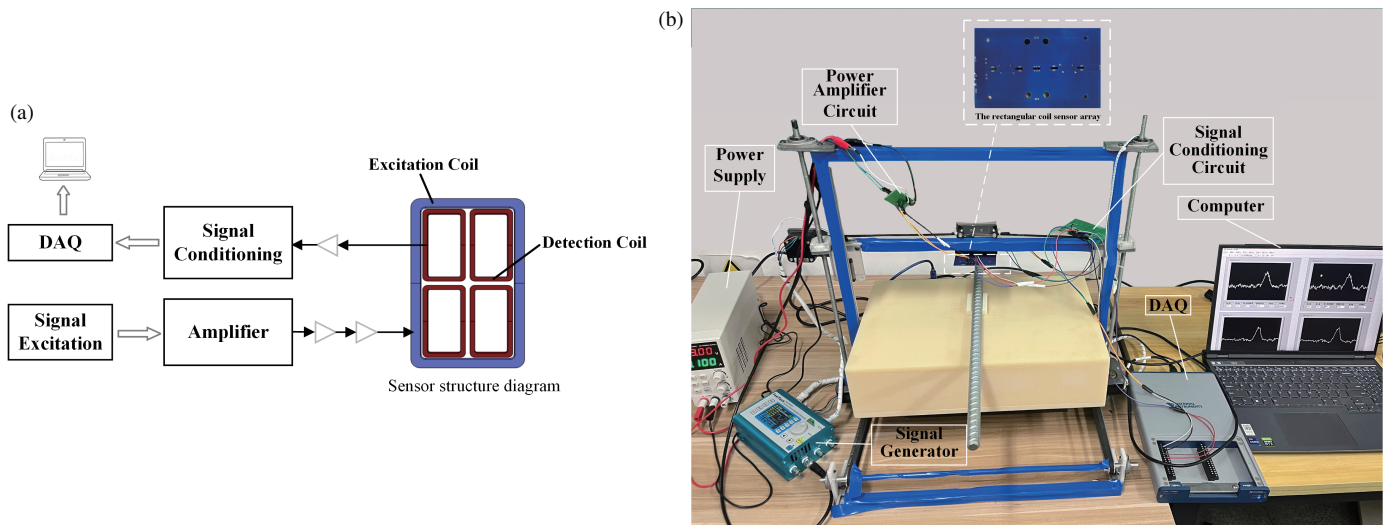


FIGURE 2. Detection System. (a) Diagram. (b) Application.

TABLE 1. Parameters of the rectangular coil.

Parameters	Exciting coil	Detecting coil
Number of turns N	200	500
Inner radius d_i (mm)	55	8
Outer radius d_o (mm)	67	20
Height h (mm)	2	2

sufficient to drive the excitation coil directly, it is necessary to design a power amplifier circuit to amplify the current flowing into the excitation coil. Metal-Oxide-Semiconductor Field-Effect Transistor (MOSFET) has the advantageous characteristics of high input resistance and low control current, and is commonly used in amplification circuits and switching circuits, so N-channel MOS is used as the main control chip for power amplification circuits. Then, the amplified current flows into the excitation coil, and the induced voltage signal is received through the detection coil. The magnitude of change is also small, which needs to be processed in two ways: amplification and filter. Therefore, a signal conditioning circuit has been designed. The signal amplifier module uses a differential amplifier circuit, which has excellent performance in anti-jamming ability, signal processing precision, and common mode interference suppression. Because of the interference of the external environment, high frequency harmonics are introduced in the experiment, so the RC low-pass filter is used to filter out these high frequency harmonic signals. Finally, the processed signal is connected to the analog channel of the NI-USB-6351 data acquisition card. At the same time, USB is used to connect the NI-USB-6351 with the computer, and the output signal is saved to the computer by configuring the trigger conditions through LabVIEW software programming.

2.2. Experimental Sample

In order to ensure the validity of the experimental results, the experiment purchased a batch of rebar with the same specifica-

tions and different diameters as the experimental samples and took the vertical distance between the coil sensor and the steel bar as the thickness of the protective layer. First, the coil sensor was fixed to the three-axis moving platform above the sample, and the experimental sample is placed vertically without any angle, and the horizontal uniform speed is moved above the sample through computer control. The number (N), diameter (D), and protective layer thickness (H) are changed, so that the detection coil picks up the corresponding voltage signal, and the signal curve is drawn. As shown in Fig. 3, the presence of peak value indicates the presence of rebar at this location. When measuring multiple rebars, the detection system in Figure 2(a) is used to determine the critical value of the large and small spacing of the rebars, and the distance between the two rebars is continuously increased with the step size of 5 mm. The number of peaks changes, then this spacing is estimated to be the critical value. Therefore, set the small spacing to 5 cm and the large spacing to 10 cm. The specific sample types and quantity distribution are shown in Table 2. A total of 2222 sets of data were collected, and the curve characteristics of some samples were extracted as shown in Fig. 3. The horizontal coordinate represents the displacement distance of the coil sensor, and the vertical coordinate represents the voltage value of the current position. l_1 and l_2 respectively indicate the spacing between the rebars. It can be seen that (1) the detection voltage is inversely proportional to the thickness of the protective layer and is proportional to the diameter; (2) When there are multiple rebars, the number of peaks varies with the spacing between the rebars. In short, it can be inferred that various rebar parameters will exhibit distinct curve characteristics.

A large number of samples are required to train the network model, and the quality of the dataset directly affects the generalization ability of the network model. Therefore, the dataset is divided into a training set and a test set. 80% of the data is used as the training set, and the remaining 20% is allocated to the test set. The test set incorporates data collected from more intricate scenarios, like multiple rebars with varying spacing as

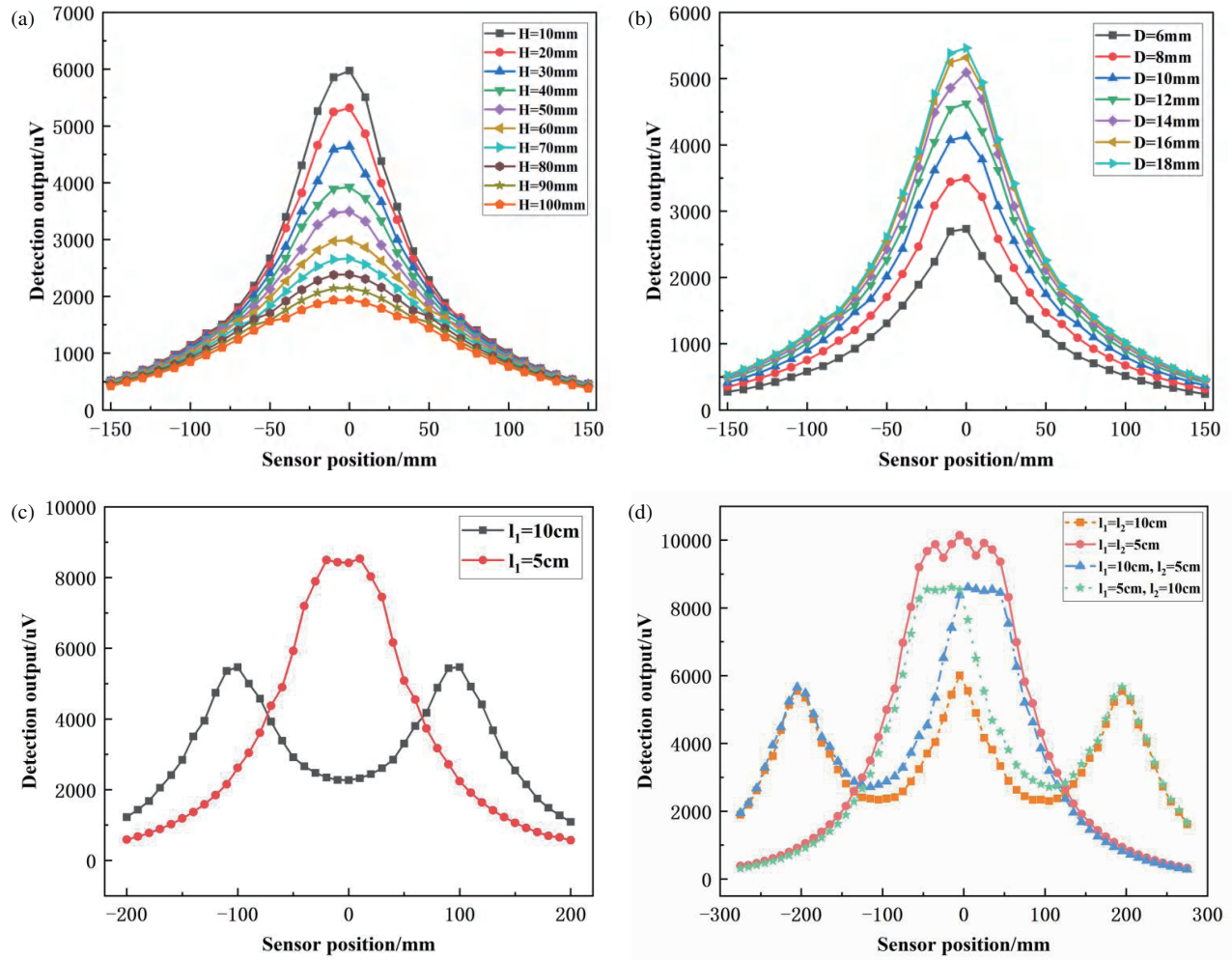

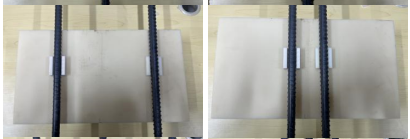
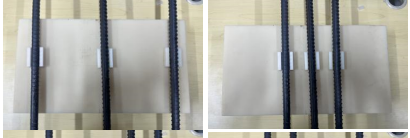



FIGURE 3. Examples of curve features of some data sets. (a) Single rebar of different thicknesses. (b) Single rebar of different diameters. (c) Two different spacing rebars. (d) Three different spacing rebars.

TABLE 2. Different sample distribution and quantity.

Type	Diagram	Quantity
Single		370
Large, Small Spacing		660
Same large, small Spacing		596
Different Spacing		596

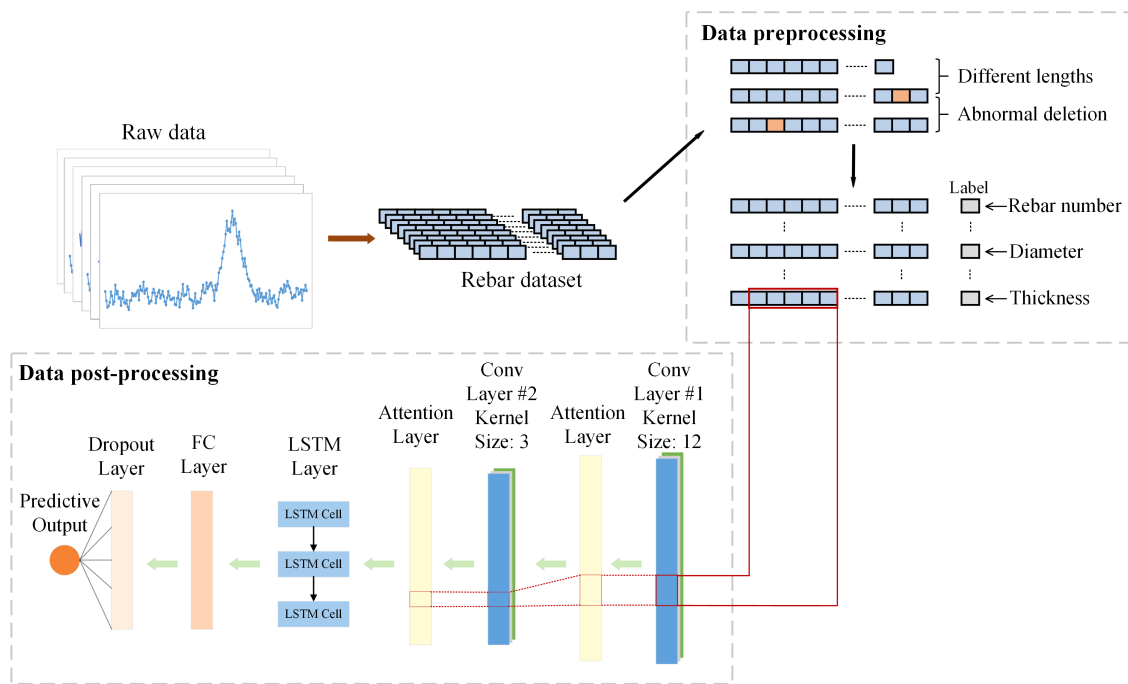


FIGURE 4. The proposed CBAM-CNN-LSTM architecture, MaxPooling layer is not included in the illustration.

shown in Table 2. This operation aims to enhance the model's performance and generalization capabilities.

3. METHOD

The deep learning model possesses a powerful fitting and expressive ability to learn complex nonlinear mappings. In this paper, the detection value and reinforced concrete parameter information are also nonlinear, so the deep learning method is employed to learn end-to-end in order to address the prediction of different parameters.

The CBAM-CNN-LSTM network model proposed in this paper consists of a preprocessing module and a post-processing module, shown in Fig. 4. The preprocessing module mainly standardizes the length of the collected experimental data and fills in any shorter sequences or missing values using linear interpolation. Additionally, it defines labels for training samples of the model, such as the number of steel bars, the size of the diameter, and the thickness of the protective layer. The post-processing module includes two types of CNN and LSTM. Since convolutional kernels of different sizes have different perception fields, smaller convolutional kernels correspond to smaller perception fields. As a result, they only capture local features, while larger kernels capture more global features. So we use two convolutional kernels with sizes of 12 and 3 to conduct the convolutional operation on the initial data in this paper, followed by a backward sliding process with a specific step size. After multiple iterations through the two-layer convolutional structure, local features are extracted. Each convolutional layer is then subjected to the activation function ReLU and the Maxpooling layer which helps aggregate and compress the features. On the one hand, due to the locally connected and translation invariant nature of CNN, the final feature in-

formation corresponds to a specific sub-region in the initial data, which lacks the full utilisation of global information. On the other hand, CNN only performs simple feature extraction through convolutional kernels, neglecting the importance of different locations and channels. Therefore, considering the need to prevent the loss of valuable information in the middle hidden layer, we propose incorporating an attention layer following the convolutional layers based on the principles of the attention mechanism [20]. This addition aims to enhance the extraction of key detection signals' expressive capabilities from different dimensions while suppressing irrelevant features. After that, the extracted feature sequences are input into the LSTM network for training to learn its temporal order. In order to capture the complex patterns and long-term dependencies between features, this paper uses three LSTM layers to improve its expressive capability. However, the network architecture is intentionally designed to avoid excessive stacking of LSTM layers. This constrain is because an abundance of such layers can result in increased model complexity, slower training speeds, and a heightened risk of overfitting. Finally, the LSTM units are iterated multiple times before being connected to the Fully Connected (FC) layer to generate the prediction results. The dropout layer is added after the FC layer to prevent overfitting by discarding part of the network with a certain probability, thus improving the generalization ability [23].

3.1. Local feature learning

3.1.1. CNN

CNN consists of an input layer, an output layer, and several hidden layers, and its structure is shown in Fig. 5. Among them, the hidden layers include a convolutional layer, an activation

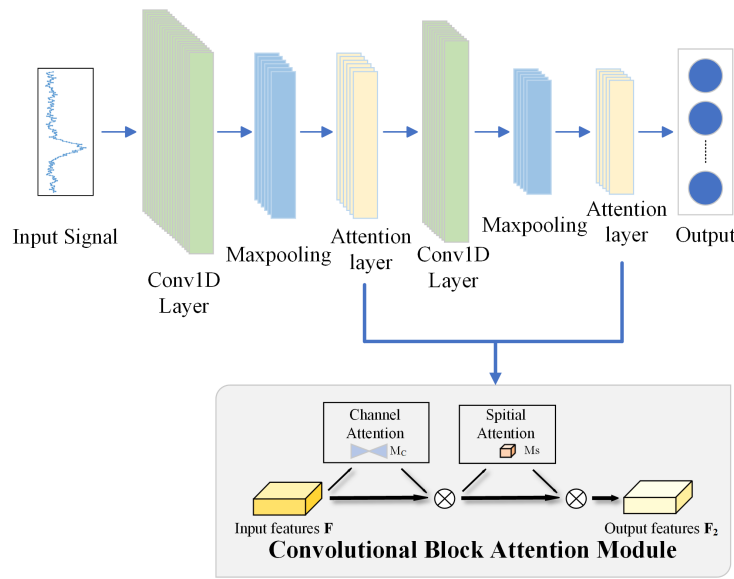


FIGURE 5. Schematic diagram of 1D CNN structure.

function, and a Maxpooling layer. In general, the convolutional layer and Maxpooling layer are used in conjunction with each other [21].

The CNN convolutional layer will rely on multiple filters to perform convolutional operations on the local features of the input signal and locally extracts the entire dataset through a fixed-size sliding window. Subsequently, under the influence of the activation function, it generates the output characteristics. The purpose of the convolution operation is to reduce the number of parameters, enhance the feature expression ability of the model, and achieve fast convergence under stochastic gradient [18]. The ReLU activation function is usually used to obtain nonlinear features, and the convolution calculation formula is

$$x_i^k = f \left(w_i^k * X^{(k-1)} + b_i^k \right) \quad (1)$$

where x_i^k is the characteristic quantity of the output of each convolution layer, f the ReLU activation function, w_i^k the weight of the convolution kernel, $*$ the convolution operation, $X^{(k-1)}$ the output of the previous layer, and b_i^k the offset.

The Maxpooling layer performs the pooling operation on the convolution feature matrix and adopts a fixed sliding window to screen the maximum value in each window region. The calculation formula is as follows.

$$p_i^{l+1}(j) = \max x_i^j(k), k \in D_j \quad (2)$$

where p_i^{l+1} is the result of Maxpooling, $x_i^j(k)$ the data within the scope of the sliding window, and D_j the pooling range.

Finally, after the calculation of multiple convolutions, activation functions, and maximum pooling, the advanced features of the detection value were obtained. In order to achieve end-to-end output, all extracted features are mapped to the sample and output through the full connection layer.

3.1.2. CBAM

The specific location and structure of the CBAM are shown in Fig. 5. It mainly integrates two attention mechanisms: channel and spatial. This module is capable of extracting features from the input data in both channel and spatial dimensions in chronological order. The feature information is then compared and modified with the original input data to generate the final feature information. The total attention process can be summarized as:

$$F_1 = M_C(F) \otimes F \quad (3)$$

$$F_2 = M_S(F_1) \otimes F_1 \quad (4)$$

where F is the input feature; F_1 is the middle feature; F_2 is the output feature; M_C and M_S are the channel and spatial attention mechanisms, respectively; \otimes indicates multiplication between elements.

Among them, the channel attention sub-module, as shown in Fig. 6(a), employs average pooling and Maxpooling operations in parallel. They can extract high-level features, and different pooling methods ensure that the extracted high-level features are more comprehensive, significantly enhancing the network's representation, instead of relying solely on individ-

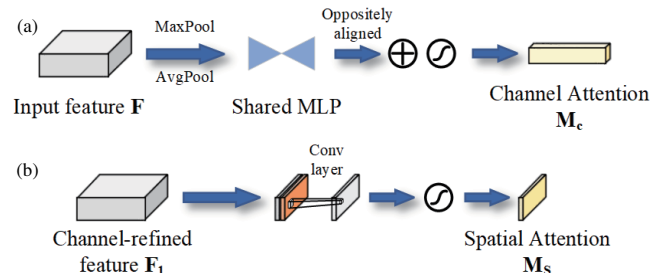


FIGURE 6. CBAM components. (a) Channel Attention Sub-module. (b) Spatial Attention Sub-module.

ual features. The spatial information of the feature maps is aggregated through a pooling operation. Subsequently, the importance of each feature channel is automatically learned by a Multilayer Perceptron (MLP), which infers a 1D-channel attention vector M_C , and it indicates the importance of each channel. Finally, the output feature vectors are merged using element-by-element summation. The specific calculation process is

$$\begin{aligned} M_c(F) &= \sigma(MLP(\text{AvgPool}(F)) + MLP(\text{MaxPool}(F))) \\ &= \sigma(W_1(W_0(F_{\text{avg}}^c)) + W_1(W_0(F_{\text{max}}^c))) \end{aligned} \quad (5)$$

where σ is a sigmoid activation function; W_0 and W_1 are the weights in the MLP and the ReLU; activation function is followed by W_0 .

The spatial attention sub-module differs from the channel attention by focusing on which locations have meaningful information. It is also complementary to the channel attention whose structure is shown in Fig. 6(a). Using the regions of valid salient information generated in channel attention, two 7×7 convolutional kernels are applied to extract features between spatial locations through the convolutional layers. This process helps infer a spatial attention map M_S , which encodes the emphasized and suppressed locations. The specific calculation process is

$$\begin{aligned} M_s(F) &= \sigma(f^{7 \times 7}([\text{AvgPool}(F); \text{MaxPool}(F)])) \\ &= \sigma(f^{7 \times 7}([F_{\text{avg}}^s; F_{\text{max}}^s])) \end{aligned} \quad (6)$$

where σ is a sigmoid activation function, and $f^{7 \times 7}$ denotes a convolution operation with a filter size of 7×7 .

Finally, since CBAM is a lightweight universal module, it can be integrated into any CNN architecture for end-to-end training, and the overhead can be ignored. This modular processing method not only shows high performance but also has extensive applicability [20].

3.2. Global Feature Learning

The core building blocks of LSTM include cell states, forgetting gates, input gates and output gates, which work together to form the unit structure of LSTM. To visualize the flow of information inside the LSTM unit, refer to Fig. 7. LSTM can

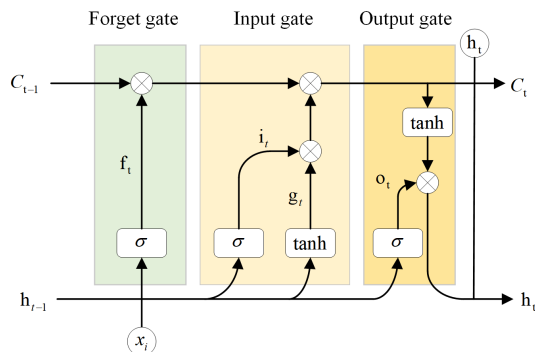


FIGURE 7. An LSTM unit structure.

regulate the state of the network unit through the forgetting gate, input gate, and output gate. It achieves adaptive learning of sequence features and performs the function of retaining useful information while eliminating unnecessary information. Among them, the feature information is extracted by CNN and transferred to LSTM. The forgetting gate controls the state of the unit by using the activation function to determine how the previous time state is updated to the current state. The input gate determines which newly received information is updated or stored by activation value and memory unit candidate state. Finally, the output gate determines which information is allowed to be output by outputting the activation value and the memory unit output value [15]. The specific calculation formula at time t is

$$i_t = \sigma(V_i x_t + W_i h_{t-1} + b_i) \quad (7)$$

$$f_t = \sigma(V_f x_t + W_f h_{t-1} + b_f) \quad (8)$$

$$\tilde{c}_t = \tanh(V_c x_t + W_c h_{t-1} + b_c) \quad (9)$$

$$c_t = f_t \otimes c_{t-1} + i_t \otimes \tilde{c}_t \quad (10)$$

$$o_t = \sigma(V_o x_t + W_o h_{t-1} + b_o) \quad (11)$$

$$h_t = o_t \otimes \tanh(c_t) \quad (12)$$

where x_t and h_* are the input and hidden state, and t represents the current time step. Respectively, V_* and W_* represent the weight matrix, and b_* is the offset of the FC layer. i_t , f_t , and o_t are the input, forget, and output gates. \otimes is a element-wise multiplication operation, and σ is a sigmoid activation function. h_t denotes the final output state.

3.3. Quantitative Analysis

In order to evaluate and compare the performance of the implemented method, we have adopted R^2 , EVS , $RMSE$, MAE as defined in Equations (13), (14), (15), and (16):

$$R^2 = 1 - \frac{\sum_{i=1}^m (y_i - \hat{y}_i)^2}{\sum_{i=1}^m (y_i - \bar{y})^2} \quad (13)$$

$$EVS = 1 - \frac{\sum_{i=1}^m (y_i - \hat{y}_i - E(y - \hat{y}))^2}{\sum_{i=1}^m (y_i - \bar{y})^2} \quad (14)$$

$$RMSE = \sqrt{\frac{\sum_{i=1}^m (y_i - \hat{y}_i)^2}{m}} \quad (15)$$

$$MAE = \frac{1}{m} \sum_{i=1}^m |y_i - \hat{y}_i| \quad (16)$$

where y_i and \hat{y}_i are the predicted and actual output of the model; \bar{y} is the average output; E is the mean; m is the number of samples.

R^2 is usually applied to measure the extent to which a regression model predicts the observed data. It represents the ratio of the variance of the data that can be explained by the model. The output of this metric lies between 0 and 1, where 1 corresponds to a perfect prediction. EVS is used to assess how well a downscaling model or feature selection model explains the

variability of the data. It reflects the proportion of data variability retained by the model, the extent to which the model is able to preserve important information about the data, and is mostly used to compare the performance of different models. It also ranges between 0 and 1, with values close to 1 indicating that the model explains the data better. *RMSE* allows for direct performance comparison, offering the advantage of imposing a larger penalty for higher error values by squaring the variance values. This prevents larger error values from disproportionately affecting the goodness-of-fit. Finally, there is *MAE*, which has relatively small impact on outliers because it uses the absolute value of the difference and is not affected by the positive or negative direction [15].

4. RESULTS AND DISCUSSION

4.1. Results

Figure 8 shows the workflow of this study. Firstly, the experimental system acquires the PECT signals with different rebar parameters. The series of collected data are labeled with the corresponding labels through preprocessing operations and trained using the CBAM-CNN-LSTM framework proposed in this paper. The specific training parameters are shown in Table 3. The losses during network training are shown in Fig. 9. After 500 training epochs, the losses of each prediction parameter tend to decrease and stabilize, indicating that the network models have all converged. In order to illustrate the su-

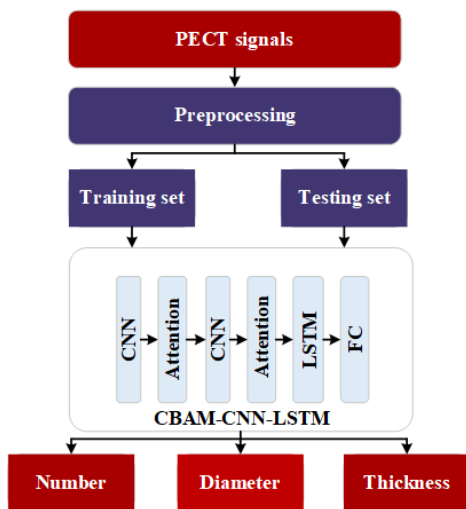


FIGURE 8. Research framework.

TABLE 3. Training parameters of the model.

Table Head	Table Column Head
Hidden layer	256
Batch size	64
Loss function	MSELoss
Optimizer	Adam
Learning rate	0.001
Dropout	0.01

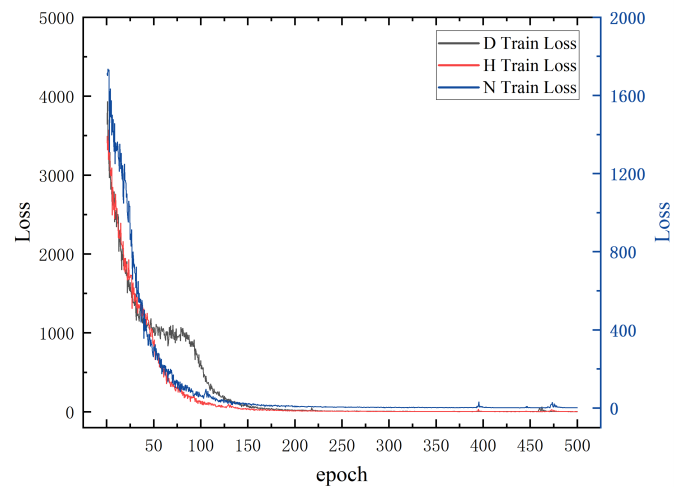


FIGURE 9. Loss during the iteration process of three parameters.

priority of the model proposed in this paper, several different deep learning network architectures including CNN, LSTM, and CNN-LSTM are employed for comparison. All models used the same data inputs, ensuring the access to identical information. In addition, all models use the same training parameters and are trained to predict the corresponding univariate variables, such as the number of rebars, diameter, or thickness of the protective layer, based on the corresponding input sequences.

In this paper, the proposed performance is evaluated on the entire test set, as shown in Figs. 10, 11, and 12. The CBAM-CNN-LSTM method proposed in this paper produces better visual results and more efficiently predicts three types of information: the quantity of objects to be measured, the diameter, and the thickness of the protective layer, than CNN, LSTM, and CNN-LSTM network models. In the traditional network model, extracting key information related to the measured objects in complex situations is challenging due to factors like neighboring rebar or signal weakening when the thickness is too large. As depicted in the prediction curves of CNN and LSTM in Figs. 10(a) and 10(b), the traditional models CNN and LSTM can only learn the information in the data in a simplistic manner. For the judgement of the number of rebars, a single rebar can make an accurate prediction. However, when there are two or more rebars, the limitations of CNN, which can only depend on the convolutional kernel for extracting local features and the lack of local feature extraction by LSTM, lead to inaccurate predictions. By combining CNN and LSTM, the advantage of CNN in extracting local features and the advantage of LSTM in capturing temporal information are fully used. This integration can improve the accuracy of predicting the quantity of two or more rebars, as shown in Fig. 10(c). However, it may also exhibit a certain level of instability. Similarly, when making judgments on diameter and thickness, the traditional CNN and LSTM predictions are also unsatisfactory, with large average errors as shown in (a) and (b) in Figs. 11 and 12. The accuracy of predicting the thickness value can be improved in the CNN-LSTM model, as shown in Fig. 10(c), and its average error is reduced by about 40% compared to the traditional model. However, unstable and fluctuating prediction abilities still occur in

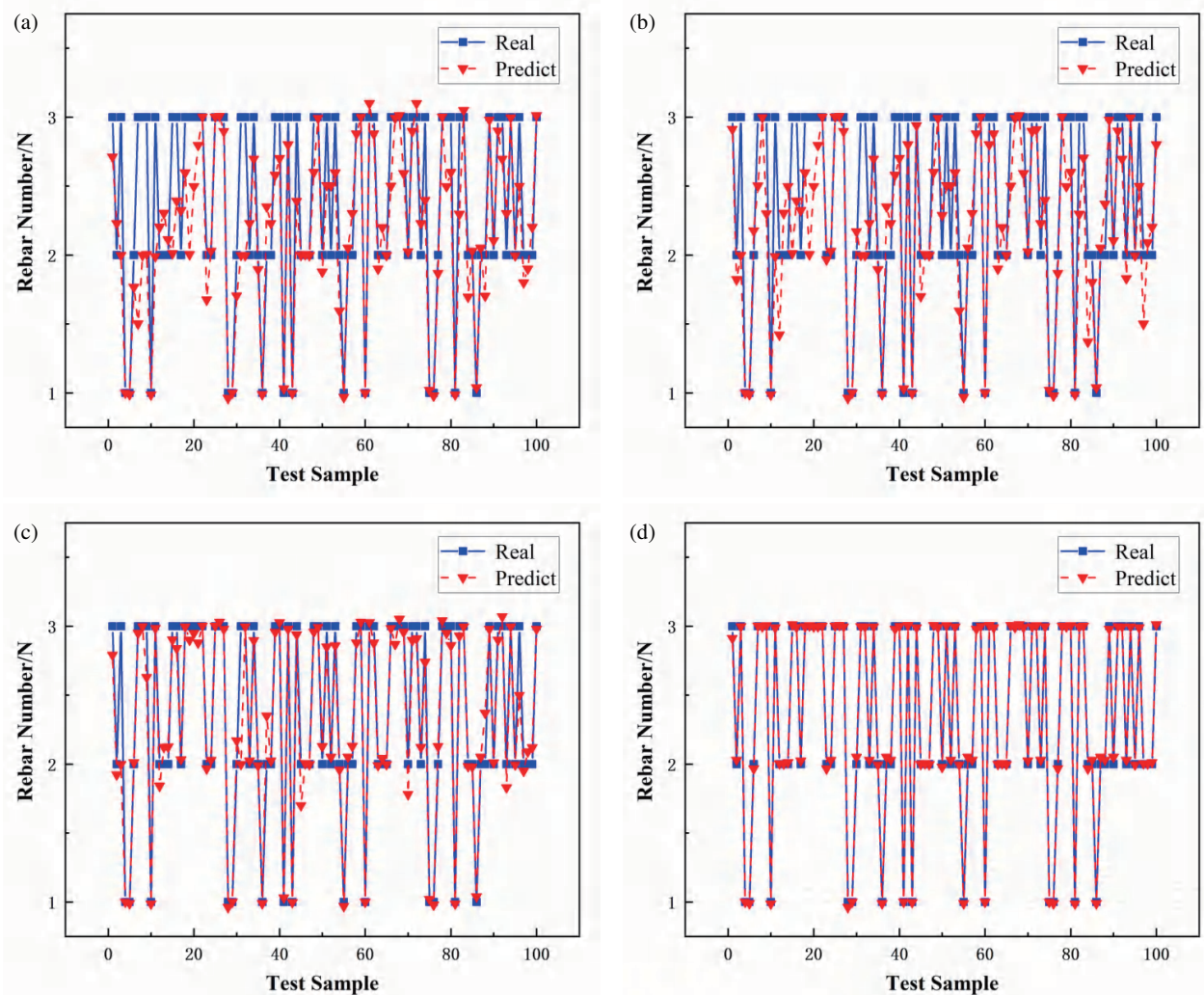


FIGURE 10. Prediction of the number of rebars. (a) CNN. (b) LSTM. (c) CNN-LSTM. (d) CBAM-CNN-LSTM.

diameter prediction, as shown in Fig. 11(c). In conclusion, the prediction accuracy of traditional CNN and LSTM models is not high. The CNN-LSTM model can address the shortcomings of the traditional models in prediction. But it lacks a certain degree of stability in overall prediction across three different parameters. This instability may reduce the reliability and credibility of the model. In contrast, using the CBAM-CNN-LSTM method proposed in this paper can extract the depth features in the data and achieve accurate and stable predictions for all three different measured information. The specific prediction graphs are shown in (d) in Figs. 10, 11, and 12.

In order to clearly quantify the different network models, quantitative evaluation of the prediction curves of the four methods in the task of predicting information about the object under test using R^2 , EVS , $RMSE$, and MAE is presented in Table 4. The results are presented in Figs. 13 and 14. The method proposed in this paper achieves the best R^2 , EVS , $RMSE$, and MAE values for all three parameter predictions. Overall, the CNN exhibits the largest feature error, followed by the LSTM and CNN-LSTM feature errors. With the incorporation of the CBAM, the fitted values of R^2 and EVS are close to 1. It can

be observed that the module allows the model to concentrate on the crucial features, enhancing the accuracy and robustness in predicting the number of rebars, diameter, and thickness. This results in a smaller error between the actual and predicted values. The biggest change is in the identification of the number of rebars, with an average error decrease of almost 50%. The least reduction is in the thickness feature, with an average error decrease of 3%. The above data illustrate that the introduction of the attention mechanism CBAM improves the overall prediction ability of the model. Simultaneously, it verifies the superiority of the CBAM-CNN-LSTM model in dealing with the time-series prediction problems.

4.2. Discussion

In this paper, an end-to-end deep learning method is proposed for predicting reinforcing bar parameter information in reinforced concrete. This method can automatically extract high-dimensional deep features directly from the original signal. It eliminates the need for complex solutions from traditional inverse solution algorithms and effectively handles the nonlinear relationship between the rebar diameter, quantity, and the

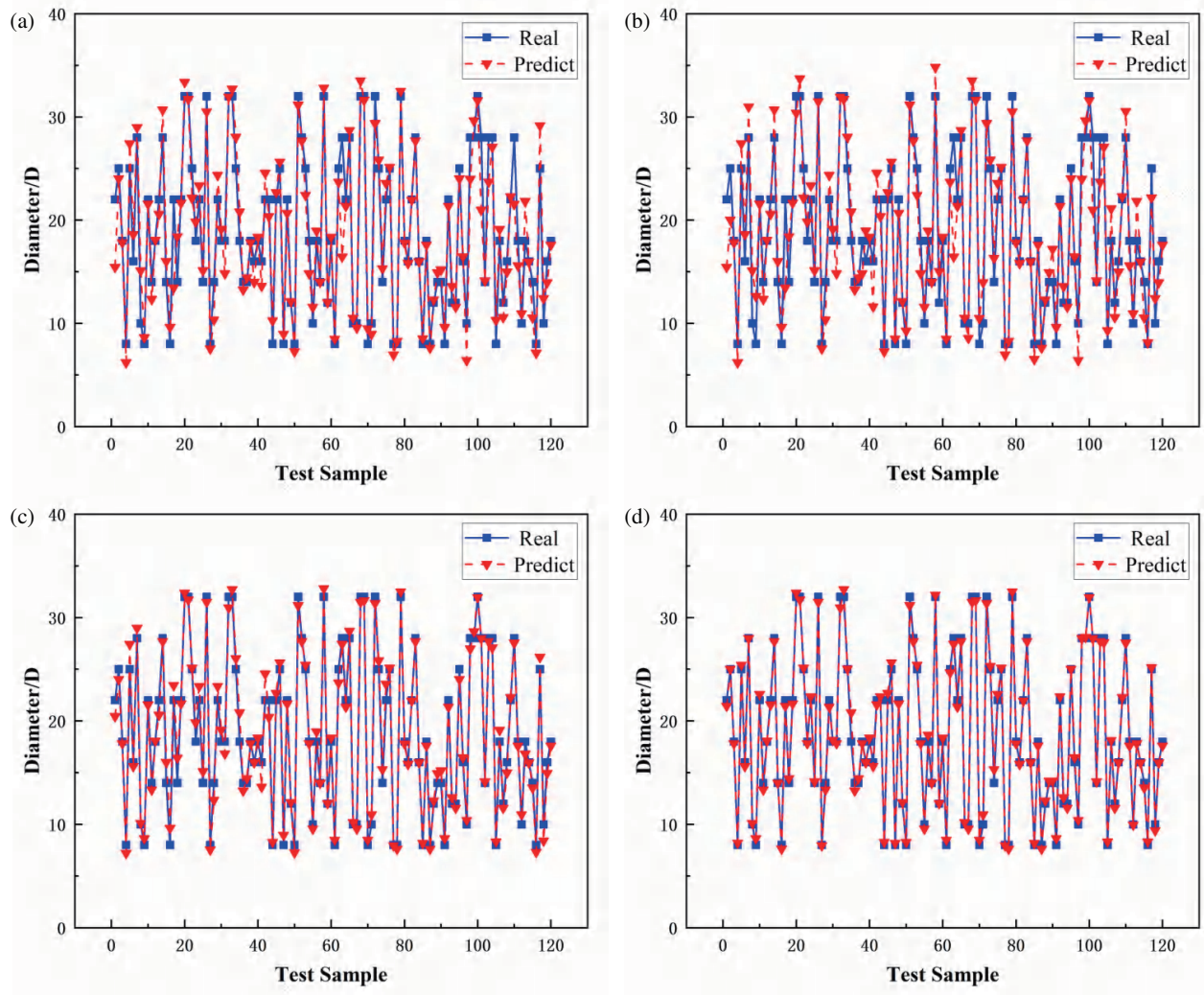


FIGURE 11. Prediction of the diameter of rebars. (a) CNN. (b) LSTM. (c) CNN-LSTM. (d) CBAM-CNN-LSTM.

TABLE 4. Training parameters of the model

Prediction parameters	Network	R^2	EVS	$RMSE$	MAE
Number/N	CNN	0.8133	0.8799	0.1016	0.2685
	LSTM	0.9161	0.9589	0.0456	0.1574
	CNN-LSTM	0.9263	0.9296	0.039	0.1684
	CBAM-CNN-LSTM	0.991	0.9928	0.0049	0.055
Diameter/D	CNN	0.7376	0.8175	5.6261	1.8291
	LSTM	0.7559	0.7574	5.2334	1.9022
	CNN-LSTM	0.8333	0.8484	3.5745	1.4784
	CBAM-CNN-LSTM	0.9143	0.9145	1.8373	1.1927
Protective Layer Height/H	CNN	0.7244	0.7456	1.8457	1.8607
	LSTM	0.8148	0.8157	1.6014	1.4897
	CNN-LSTM	0.9801	0.9814	1.0316	0.9054
	CBAM-CNN-LSTM	0.9968	0.9975	0.8492	0.8838

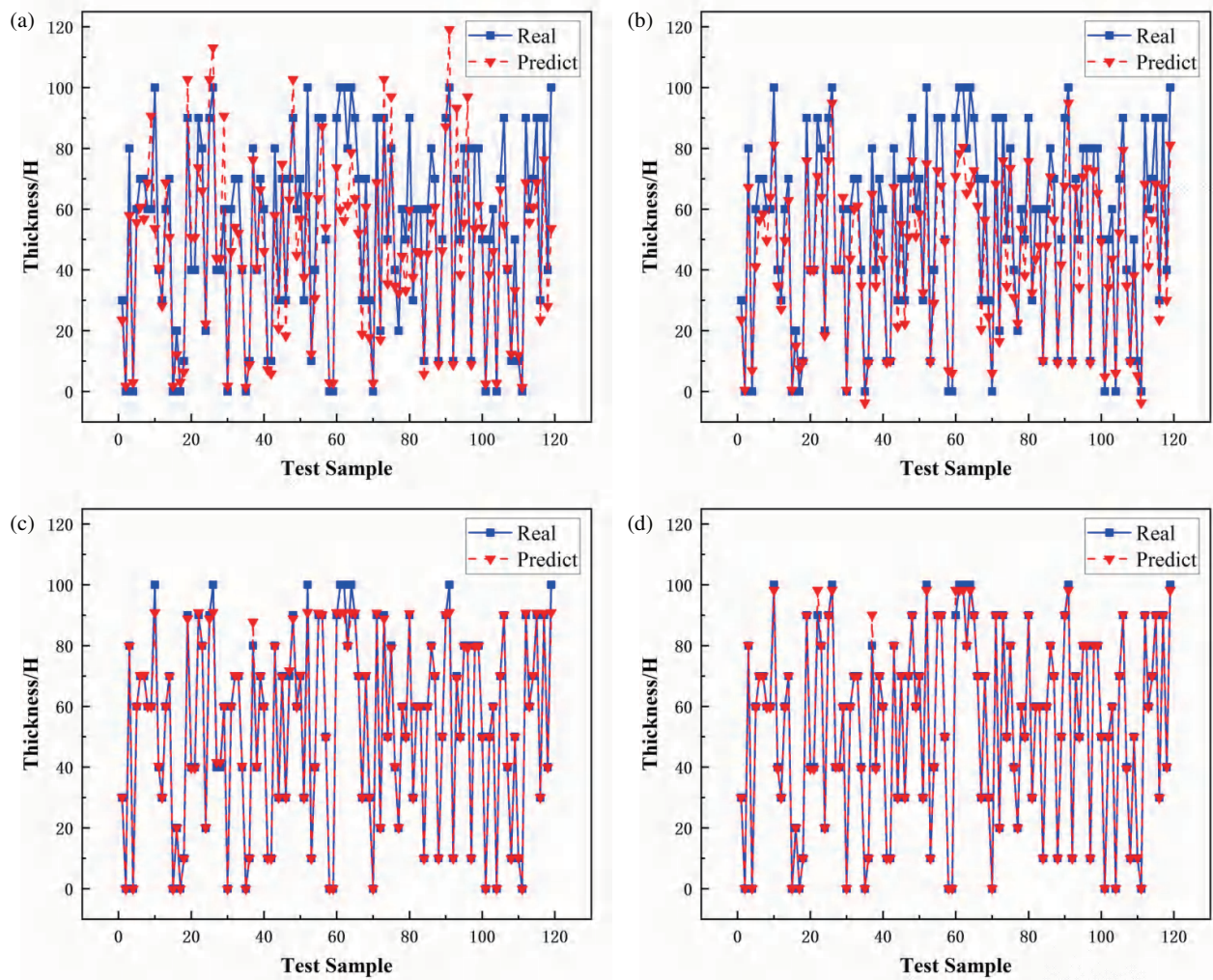


FIGURE 12. Prediction of the thickness of the protective layer of the rebars. (a) CNN. (b) LSTM. (c) CNN-LSTM. (d) CBAM-CNN-LSTM.

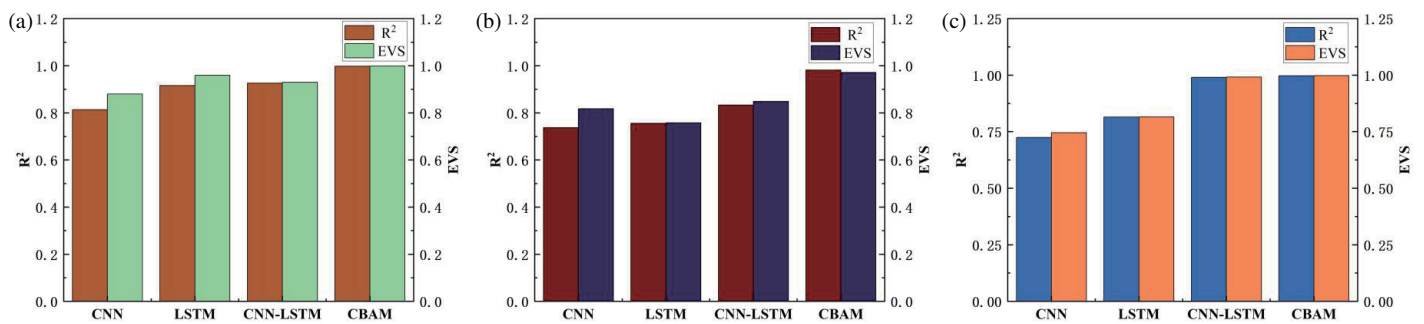


FIGURE 13. Comparison of R_2 and EVS of four different network models. (a) Number/ N . (b) Diameter/ D . (c) Protective layer thickness/ H .

height of the protective layer, and electromagnetic signals. This capability surpasses what traditional machine learning methods can achieve. There are other reasons that affect the relationship mapping between parameter information and PECT signals. For example, during the measurement process, it may be observed that the impact of rebar diameter on the PECT signal and the effect of protective layer thickness on the PECT signal are interconnected. This interconnection may lead to chal-

lenges in accurately determining the protective layer thickness or the rebar diameter when using a multi-input multi-output network model. Based on this conjecture, this paper adopts the same network model to implement multi-input and single-output modes for predicting the number of rebars, diameters, and the thickness of the protective layer. It has been proven to have a certain identification effect.

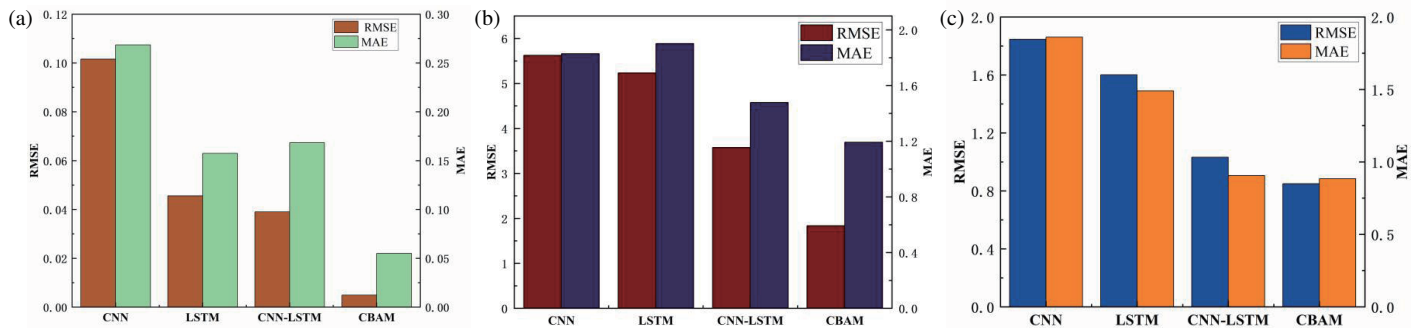


FIGURE 14. Comparison of RMSE and MAE of four different network models. (a) Number/ N . (b) Diameter/ D . (c) Protective layer thickness/ H .

5. CONCLUSION

An intelligent prediction method, CBAM-CNN-LSTM, based on PECT signals is proposed for solving the inverse problem of determining the diameter, number, and thickness of the protective layer of steel bars in reinforced concrete. The collected PECT signals are directly used to automatically extract the parameter information prediction features using the deep learning method. The experimental data are used to test the model and verify its effectiveness, and the main conclusions are as follows:

(1) The model can accept the unprocessed PECT time series signals directly, express the features of the original data through deeply learning, thus overcoming the shortcomings of manual feature extraction and prediction accuracy. This enables the end-to-end prediction of reinforced concrete parameter information.

(2) By incorporating the attention mechanism CBAM into CNN-LSTM, its performance is compared and analyzed against traditional CNN, LSTM, and CNN-LSTM. The results show that emphasizing key features can enhance the performance of the whole network model, and it has a good effect on the prediction of PECT signals. Especially in terms of the overall prediction results, all the methods proposed in this paper demonstrate high accuracy and stability.

(3) The model adopts a multi-input, single-output mode to predict the corresponding parameters separately. This approach helps the model eliminate many data elements that are not related to the output during computation. As a result, the overall computational demand of the model is small, and computation is fast so that it can be implemented in embedded systems for real world applications.

ACKNOWLEDGEMENT

This research was funded by National Natural Science Foundation of China under Grant (62071328).

REFERENCES

- [1] Hassani, S. and U. Dackermann, "A systematic review of advanced sensor technologies for non-destructive testing and structural health monitoring," *Sensors*, Vol. 23, No. 4, 2204, Feb. 2023.
- [2] El Masri, Y. and T. Rakha, "A scoping review of non-destructive testing (NDT) techniques in building performance diagnostic inspections," *Construction and Building Materials*, Vol. 265, 120542, 2020.
- [3] Clark, M. R., D. M. McCann, and M. C. Forde, "Application of infrared thermography to the non-destructive testing of concrete and masonry bridges," *NDT & E International*, Vol. 36, No. 4, 265–275, 2003.
- [4] Wicker, M., B. P. Alduse, and S. Jung, "Detection of hidden corrosion in metal roofing shingles utilizing infrared thermography," *Journal of Building Engineering*, Vol. 20, 201–207, 2018.
- [5] Wang, J., K. Chen, H. Liu, J. Zhang, W. Kang, S. Li, P. Jiang, Q. Sui, and Z. Wang, "Deep learning-based rebar clutters removal and defect echoes enhancement in GPR images," *IEEE Access*, Vol. 9, 87 207–87 218, 2021.
- [6] Liu, H., C. Lin, J. Cui, L. Fan, X. Xie, and B. F. Spencer, "Detection and localization of rebar in concrete by deep learning using ground penetrating radar," *Automation in Construction*, Vol. 118, 103279, 2020.
- [7] Meng, T., Y. Tao, Z. Chen, J. R. S. Avila, Q. Ran, Y. Shao, R. Huang, Y. Xie, Q. Zhao, Z. Zhang, *et al.*, "Depth evaluation for metal surface defects by eddy current testing using deep residual convolutional neural networks," *IEEE Transactions on Instrumentation and Measurement*, Vol. 70, 1–13, 2021.
- [8] Sha, J., M. Fan, and B. Ye, "Intelligent hardness prediction of bearing rings using pulsed eddy current testing," *IEEE Sensors Journal*, Vol. 22, No. 23, 23 320–23 327, Dec. 2022.
- [9] Tamhane, D., J. Patil, S. Banerjee, and S. Tallur, "Feature engineering of time-domain signals based on principal component analysis for rebar corrosion assessment using pulse eddy current," *IEEE Sensors Journal*, Vol. 21, No. 19, 22 086–22 093, 2021.
- [10] Chen, X., J. Li, and Z. Wang, "Inversion method in pulsed eddy current testing for wall thickness of ferromagnetic pipes," *IEEE Transactions on Instrumentation and Measurement*, Vol. 69, No. 12, 9766–9773, 2020.
- [11] Heng, W., L. Xiaoyi, D. Zhaolin, and D. Youquan, "Measurement method of reinforcement diameter and buried depth based on GA-BP neural network," *Journal of Chongqing University of Science and Technology (Natural Sciences Edition)*, Vol. 25, 97–102, 2023.
- [12] Chunyi, L., J. Yu, Y. Zhongdong, D. Shuangson, Z. Zhanlong, and Q. Kecheng, "Detection method of rebar in concrete diameter based on improved grey wolf optimizer-based SVR," *Computer Science*, Vol. 49, 228–233, 2022.
- [13] Ahmed, H., H. M. La, and K. Tran, "Rebar detection and localization for bridge deck inspection and evaluation using

- deep residual networks,” *Automation in Construction*, Vol. 120, 103393, 2020.
- [14] Petmezas, G., K. Haris, L. Stefanopoulos, V. Kilintzis, A. Tzavelis, J. A. Rogers, A. K. Katsaggelos, and N. Maglaveras, “Automated atrial fibrillation detection using a hybrid CNN-LSTM network on imbalanced ECG datasets,” *Biomedical Signal Processing and Control*, Vol. 63, 102194, 2021.
- [15] Elmaz, F., R. Eyckerman, W. Casteels, S. Latré, and P. Hellinckx, “CNN-LSTM architecture for predictive indoor temperature modeling,” *Building and Environment*, Vol. 206, 108327, Dec. 2021.
- [16] Kim, T.-Y. and S.-B. Cho, “Predicting residential energy consumption using CNN-LSTM neural networks,” *Energy*, Vol. 182, 72–81, Sep. 2019.
- [17] Hou, J., Y. Wang, J. Zhou, and Q. Tian, “Prediction of hourly air temperature based on CNN–LSTM,” *Geomatics, Natural Hazards and Risk*, Vol. 13, No. 1, 1962–1986, 2022.
- [18] Yan, R., J. Liao, J. Yang, W. Sun, M. Nong, and F. Li, “Multi-hour and multi-site air quality index forecasting in Beijing using CNN, LSTM, CNN-LSTM, and spatiotemporal clustering,” *Expert Systems with Applications*, Vol. 169, 114513, 2021.
- [19] Zhao, J., X. Mao, and L. Chen, “Speech emotion recognition using deep 1D & 2D CNN LSTM networks,” *Biomedical Signal Processing and Control*, Vol. 47, 312–323, Jan. 2019.
- [20] Woo, S., J. Park, J.-Y. Lee, and I. S. Kweon, “Cbam: Convolutional block attention module,” in *Proceedings of the European Conference on Computer Vision (ECCV)*, 3–19, 2018.
- [21] Tsopelas, N. and N. J. Siakavellas, “Performance of circular and square coils in electromagnetic-thermal non-destructive inspection,” *NDT & E International*, Vol. 40, No. 1, 12–28, 2007.
- [22] Bao, T., S. A. R. Zaidi, S. Xie, P. Yang, and Z.-Q. Zhang, “A CNN-LSTM hybrid model for wrist kinematics estimation using surface electromyography,” *IEEE Transactions on Instrumentation and Measurement*, Vol. 70, 1–9, 2020.
- [23] Thomas, J. B., S. G. Chaudhari, K. V. Shihabudheen, and N. K. Verma, “CNN-based transformer model for fault detection in power system networks,” *IEEE Transactions on Instrumentation and Measurement*, Vol. 72, 1–10, 2023.